^{11}B Chemical Shift Anisotropies in Borates from ^{11}B MAS, MQMAS, and Single-Crystal NMR Spectroscopy

Michael Ryan Hansen,[†] Thomas Vosegaard,[‡] Hans J. Jakobsen,[†] and Jørgen Skibsted*[,†]

Instrument Centre for Solid-State NMR Spectroscopy, Department of Chemistry, University of Aarhus, DK-8000 Aarhus C, Denmark, and Interdisciplinary Nanoscience Center (iNANO) and Laboratory for Biomolecular NMR Spectroscopy, Department of Molecular and Structural Biology, University of Aarhus, DK-8000 Aarhus C, Denmark.

Received: July 30, 2003; In Final Form: October 21, 2003

^{11}B chemical shift anisotropies (CSAs) have been obtained for tetrahedral and trigonal boron sites in tetraphenyl borates, datolite ($CaBSiO_4(OH)$), danburite ($CaB_2Si_2O_8$), colemanite ($CaB_3O_4(OH)_3 \cdot H_2O$), borax ($Na_2B_4O_7 \cdot 10H_2O$), and $Li_2B_4O_7$ from solid-state ^{11}B NMR spectra recorded at 14.1 T. These parameters along with ^{11}B quadrupole couplings and the relative orientation of the quadrupole coupling and CSA tensors have been determined from either the manifold of spinning sidebands observed for the satellite transitions in ^{11}B MAS NMR spectra or single-crystal NMR spectra of the satellite transitions. Furthermore, the potential of the MQMAS experiment for determination of small ^{11}B CSAs is illustrated for the trigonal boron site in $Li_2B_4O_7$. The ^{11}B single-crystal NMR spectra of the satellite transitions are strongly dominated by the first-order quadrupolar interaction, which may prevent a direct determination of small CSAs. However, an improved precision of the CSA parameters and the Euler angles, describing the relative orientation of the CSA and quadrupole coupling tensors, are achieved from analysis of rotation plots for the sum frequencies of the $m = {}^1/_2 \leftrightarrow m = {}^3/_2$ and $m = -{}^1/_2 \leftrightarrow m = -{}^3/_2$ transitions, which are influenced only by the first-order CSA and the second-order quadrupolar interactions. The ^{11}B CSA parameters determined in this work show that tetrahedrally coordinated boron in borates possess shift anisotropies ($\delta_\sigma = \delta_{iso} - \delta_{zz}$) of magnitude $|\delta_\sigma|$ less than 10 ppm.

Introduction

^{11}B NMR spectroscopy is a well-established analytical tool in several areas of the diverse structural chemistry of boron. In particular, solid-state ^{11}B NMR has been a popular technique in the structural characterization of boron-containing glasses, because early work has shown that trigonal (BO_3) and tetrahedrally coordinated (BO_4) boron can be distinguished by their ^{11}B quadrupole coupling parameters (C_Q and η_Q),[1−3] thereby allowing a determination of the relative fraction of these two boron sites for different materials. For boron in borates, boron-containing glasses, and minerals, the ^{11}B quadrupole constants are smaller than 1 MHz for BO_4 tetrahedra whereas BO_3 units possess quadrupole couplings in the range $2.4 \lesssim C_Q \lesssim 3.0$ MHz.[3−9] Moreover, for these materials the BO_3 units exhibit isotropic chemical shifts in the range $12 \lesssim \delta_{iso} \lesssim 25$ ppm whereas BO_4 tetrahedra resonate at lower frequencies in the range $-4 \lesssim \delta_{iso} \lesssim 6$ ppm. Thus, separate resonances for BO_3 and BO_4 species can generally be achieved using high-speed ^{11}B MAS NMR at high magnetic fields ($B \gtrsim 9.4$ T), which facilitates the quantification of these species.[5,10] ^{11}B quadrupole coupling parameters have primarily been reported for BO_3 sites, because these parameters are easily extracted from the second-order quadrupolar line shapes observed for the central transition in either static-powder or MAS NMR spectra.[4,5] The small quadrupole couplings associated with BO_4 tetrahedra do not result in such characteristic line shapes for the central transition. Thus, these parameters have been determined for BO_4 units for only a limited number of borates or borate minerals from either the manifold of spinning sidebands (ssbs) in MAS NMR spectra of the satellite transitions[11−13] or from single-crystal (SC) NMR.[14,15]

The increase in commercially available magnetic field strengths has directed attention to the influence of even small chemical shift anisotropies (CSAs) for a number half-integer spin quadrupolar nuclei. The effect of the CSA becomes increasingly important at high magnetic fields, because this interaction is proportional to the magnetic field strength whereas line broadening effects from the second-order quadrupole interaction scale inversely with increasing B_0. Recently, ^{11}B CSAs have been reported for tricoordinate boron in trimesitylborane,[16] triphenylborate,[16] and hexamethylborazine,[17] for a number of crystalline borates,[9] and for two decamethylcyclopentadienyl boron complexes[18] from ^{11}B static-powder and MAS NMR spectra of the central transition observed at moderate (8.46−9.4 T) and high (17.6−18.8 T) magnetic field strengths. The largest shift anisotropies ($\delta_\sigma = \delta_{iso} - \delta_{zz}$) are reported for bis(pentamethylcyclopentadienyl)methylborane ($\delta_\sigma = 91.3$ ppm),[18] and trimesitylborane ($\delta_\sigma = 80.7$ ppm),[16] whereas significant smaller shift anisotropies ($\delta_\sigma = 10-22$ ppm) are observed for the borates B_2O_3, $Cs_2O \cdot 9B_2O_3$, $CaO \cdot B_2O_3$, $2MgO \cdot B_2O_3$, and $La_2O_3 \cdot B_2O_3$.[9] Obviously, the large CSAs observed for the two former compounds reflect highly distorted environments for the tricoordinate boron in these compounds. This distortion is also reflected by the quadrupole coupling constants, which are determined to be $C_Q = 4.52$ MHz for bis(pentamethylcyclo-

* Corresponding author. Fax: +45 8619 6199. Phone: +45 8942 3900. E-mail: jskib@chem.au.dk.
[†] Department of Chemistry, University of Aarhus.
[‡] Department of Molecular and Structural Biology, University of Aarhus.

10.1021/jp030939h CCC: $27.50
Published on Web 12/30/2003

pentadienyl)methylborane[18] and $C_Q = 4.75$ MHz for trimesitylborane.[16] However, considering the high degree of symmetry of the electronic charge distribution surrounding the boron nucleus in BO_4 units, it is expected that borates including tetrahedrally coordinated boron should possess small CSAs of the order $|\delta_\sigma| \approx 5-10$ ppm. Thus, determination of ^{11}B CSAs along with the quadrupole coupling parameters for BO_4 tetrahedra in borates represents quite a challenge using the NMR techniques commonly employed in solid-state ^{11}B NMR. It is noted that the quadrupole coupling and CSA parameters represent two different sources of structural information, because the origins of these interactions are reflected in a different manner by the local electronic environment. The quadrupole coupling depends only on the ground state of the local electronic field whereas the CSA also includes higher order interactions, reflecting the excited states of the electronic field.

In this work we report the determination of ^{11}B CSAs along with the quadrupole couplings for tetrahedrally coordinated boron in a number of tetraphenylborates, tetraborates, and the boron-containing minerals datolite ($CaBSiO_4(OH)$), danburite ($CaB_2Si_2O_8$), and colemanite ($CaB_3O_4(OH)_3 \cdot H_2O$). The parameters are determined from either ^{11}B MAS NMR spectra of the satellite transitions, SC NMR, or MQMAS spectra recorded at a magnetic field of 14.1 T.

Experimental Section

The tetraphenylborates $MB(C_6H_5)_4$ (M = NH_4, Na, K, Rb, Cs), $Li_2B_4O_7$, and $Na_2B_4O_7 \cdot 10H_2O$ (borax) were purchased from Aldrich (Milwaukee, WI) and used without further purification. For the single-crystal NMR study of borax a suitable-sized crystal ($\sim 2.5 \times 2.0 \times 2.5$ mm^3) was obtained by slow evaporation of an aqueous solution of $Na_2B_4O_7 \cdot 10H_2O$. Single crystals and powders of mineral samples of datolite (Sibiria, Russia), danburite (Chareas, Mexico), and colemanite (Bursa, Turkey) were kindly provided by the Department of Geology, University of Aarhus, and the Geological Museum, University of Copenhagen. The structures and purities of these samples were confirmed by ^{29}Si MAS NMR and/or powder X-ray diffraction.

The solid-state ^{11}B NMR experiments were performed at ambient temperature on a Varian INOVA-600 (14.1 T) spectrometer ($\nu_L = 192.48$ MHz). The ^{11}B MAS NMR spectra of the satellite transitions were recorded using either a 7 mm CP/MAS probe from DOTY Scientific Inc. or a home-built CP/MAS probe for 4 mm o.d. rotors and with transmission-line tuning (TLT) for the high-frequency channel. The spectra employed a short rf pulse width $\tau_p = 0.5-1.0$ μs for a rf field strength of $\gamma B_1/2\pi \approx 40$ kHz (7 mm probe) or $\gamma B_1/2\pi \approx 65$ kHz (4 mm probe) and ^{1}H decoupling ($\gamma B_2/2\pi \approx 50$ kHz for both probes). The MQMAS experiment was performed using a home-built 4 mm MAS probe and $\gamma B_1/2\pi \approx 120$ kHz. The magic angle was adjusted by optimization of the line widths for the spinning sidebands in the ^{23}Na MAS NMR spectrum of $NaNO_3$ whereas stable spinning frequencies were achieved using the Varian rotor-speed controller. The SC NMR spectra were recorded using a double-tuned (X-^{1}H) SC NMR probe equipped with a two-axis goniometer and a 3 turn 3.8 mm i.d. rf coil,[19] designed particularly for improving the sensitivity of the NMR response for small crystals.[20] This design employs only two axes of rotation (*a* and *b*), which are separated by an angle of $\sim 39°$. Rotation of the crystal is fully automated and controlled by the host computer of the spectrometer via a home-built interface.[19,21] This setup ensures a high precision ($\pm 0.3°$) in setting the rotation angle (θ). For each rotation axis, 41 spectra were recorded following an increment in rotation angle of 9° and employing single-pulse excitation ($\tau_p = 0.5-1.0$ μs for $\gamma B_1/2\pi \approx 50$ kHz), ^{1}H decoupling ($\gamma B_2/2\pi \approx 60$ kHz), a spectral width of 0.5, 1.0, or 3.0 MHz, and between 40 and 448 scans with repetition delays in the range of 4−30 s.

The quadrupole coupling and CSA parameters are defined as

$$C_Q = \frac{eQV_{zz}}{h} \qquad \eta_Q = \frac{V_{yy} - V_{xx}}{V_{zz}} \tag{1}$$

$$\delta_{iso} = \frac{1}{3}\mathrm{Tr}(\delta) \qquad \delta_\sigma = \delta_{iso} - \delta_{zz} \qquad \eta_\sigma = \frac{\delta_{xx} - \delta_{yy}}{\delta_\sigma} \tag{2}$$

using the convention $|\lambda_{zz} - {}^1/_3\mathrm{Tr}(\lambda)| \geq |\lambda_{xx} - {}^1/_3\mathrm{Tr}(\lambda)| \geq |\lambda_{yy} - {}^1/_3\mathrm{Tr}(\lambda)|$ for the principal elements ($\lambda_{ii} = V_{ii}$, δ_{ii}) of the electric field gradient (**V**) and CSA ($\boldsymbol{\delta}$) tensors. The relative orientation of the two tensors is described by the Euler angles ψ, χ, and ξ,[22,23] which correspond to positive rotations of the CSA tensor around δ_{zz} (ψ), the new δ_{yy} (χ), and the final δ_{zz} (ξ) axis. Simulations,[24,25] least-squares optimizations, and error analysis[26] of the experimental MAS NMR spectra were performed using the *STARS* software whereas the analysis of the SC NMR spectra employed the *ASICS*[21] or the *SIMPSON*[27] and *SIMMOL*[28,29] software packages. The ^{11}B isotropic chemical shifts are in ppm relative to neat $F_3B \cdot O(CH_2CH_3)_2$ employing a 0.1 M H_3BO_3 aqueous solution ($\delta_{iso} = 19.6$ ppm)[9,30] as a secondary reference sample.

Results and Discussion

The determination of ^{11}B CSA parameters for the borates studied in this work is described in the following paragraphs in order of increasing complexity of the ^{11}B NMR spectra and of the crystal structures. Where possible, the ^{11}B quadrupole coupling parameters and isotropic chemical shifts are compared with ^{11}B NMR data reported earlier in the literature.

Tetraphenylborates. The slow-speed ($\nu_R = 1.0$ kHz) ^{11}B MAS NMR spectrum of $NH_4B(C_6H_5)_4$ (Figure 1a) illustrates a manifold of ssbs from the satellite transitions for a single ^{11}B site in $NH_4B(C_6H_5)_4$, in agreement with the crystal structure reported from neutron diffraction.[31] The envelope of ssbs exhibits significant asymmetries in ssb intensities around the central transition, which is most clearly observed in the spectral regions for the singularities ("horns", ± 5 kHz) and the outer edges (± 10 to ± 15 kHz). A minor variation is also observed in the line widths for the individual ssbs and thus, a stick-plot of ssb intensities is shown in Figure 1b for comparison with the simulated spectra. The distinct asymmetries in the spectrum cannot arise from ^{11}B−^{11}B or ^{11}B−^{1}H dipolar couplings, considering the long ^{11}B−^{11}B distance (~ 8.8 Å) in $NH_4B(C_6H_5)_4$ and the use of high-power ^{1}H decoupling. Thus, the spectrum in Figure 1a gives clear evidence for a contribution from a ^{11}B CSA to the ssb intensities. The manifold of ssb intensities in Figure 1b is simulated by consideration of the average Hamiltonians for the first-order quadrupolar ($\bar{\mathscr{H}}_Q^{(1)}$) and CSA ($\bar{\mathscr{H}}_\sigma^{(1)}$) interactions, employing the same approach as used in earlier studies of CSAs for half-integer spin quadrupolar nuclei.[22,25,26] This approach combined with least-squares fitting results in the simulated manifold of ssbs in Figure 1d, which corresponds to the ^{11}B quadrupole coupling constant, shift anisotropy (δ_σ), and isotropic chemical shift listed in Table 1 for $NH_4B(C_6H_5)_4$. The clear observation of a ^{11}B CSA is also apparent from a comparison of the experimental and simulated spectra in Figure 1a,d, respectively, with the simulated spectrum in Figure 1c,

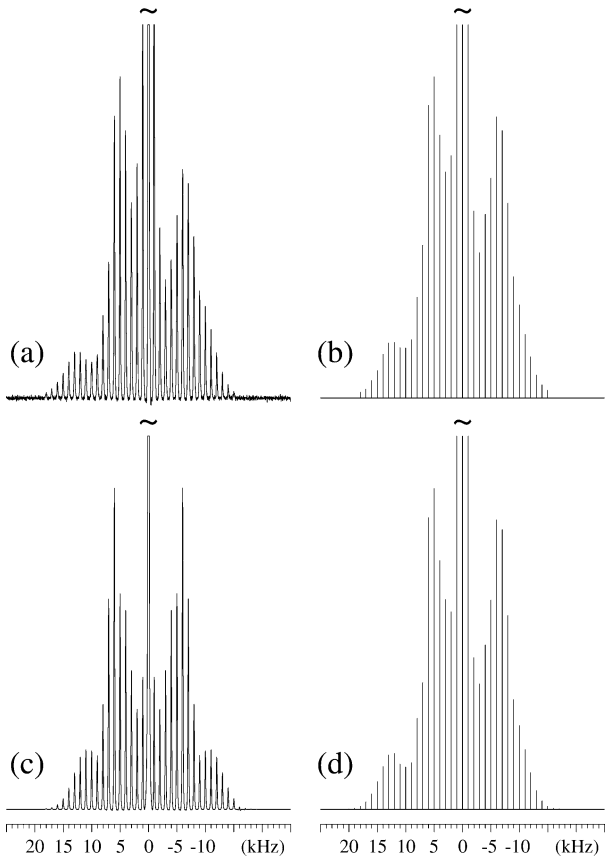

Figure 1. (a) ^{11}B MAS NMR spectrum (14.1 T) of $NH_4B(C_6H_5)_4$ employing ^{1}H decoupling, a spinning speed of 1.0 kHz, a relaxation delay of 10 s, and 1024 scans. (b) Stick plot of integrated intensities for the center band and ssbs of the experimental spectrum shown in (a). (d) Stick plot of ssb intensities resulting from least-squares fitting to the ssbs in (b) and corresponding to the C_Q, δ_σ, and δ_{iso} values listed in Table 1 for $NH_4B(C_6H_5)_4$. The simulation employs the constraints, $\eta_Q = \eta_\sigma = 0.0$ and coincidence of the quadrupole coupling and CSA tensors, imposed by the crystal structure for $NH_4B(C_6H_5)_4$. For comparison, (c) illustrates a simulated spectrum using the parameters in Table 1 but disregarding the effect from the CSA. The center band for the central transition and its first-order ssbs have been cutoff at approximately one-fifth of the total height for the centerband in (a)−(d).

TABLE 1: ^{11}B Quadrupole Coupling Constants (C_Q), Shift Anisotropies (δ_σ), and Isotropic Chemical Shifts (δ_{iso}) from ^{11}B MAS NMR Spectra of Tetraphenylborates[a]

compound	δ_{iso} (ppm)	C_Q (kHz)	δ_σ (ppm)
$NH_4B(C_6H_5)_4$	-7.9 ± 0.3	29.4 ± 0.7	-7.9 ± 0.5
$NaB(C_6H_5)_4$	-9.2 ± 0.3	34.9 ± 1.2	-7.9 ± 1.0
$KB(C_6H_5)_4$	-8.1 ± 0.3	28.2 ± 0.8	-7.5 ± 0.6
$RbB(C_6H_5)_4$	-7.8 ± 0.4	29.9 ± 0.9	-7.2 ± 0.6
$CsB(C_6H_5)_4$	-7.8 ± 0.4	35.0 ± 0.5	-5.7 ± 0.8

[a] The C_Q and δ_σ parameters are obtained from optimizations which employ the contraint $\eta_Q = \eta_\sigma = 0.0$ and thereby coincidence of the quadrupole coupling and CSA tensors, as imposed by the tetragonal crystal structure.

which is obtained by neglecting the effect of a ^{11}B CSA. The extremely small C_Q value demonstrates high symmetry of the local environment for the tetrahedrally coordinated boron site in $NH_4B(C_6H_5)_4$, in accord with its crystal structure (tetragonal, space group $I\bar{4}2m$),[31] where the boron atom is situated on a 4-fold axis. This implies axial symmetry of the quadrupole coupling and CSA tensors, in agreement with the result from least-squares optimizations where $\eta_Q \approx \eta_\sigma \approx 0$ and almost coincidence of the quadrupole coupling and CSA tensors are

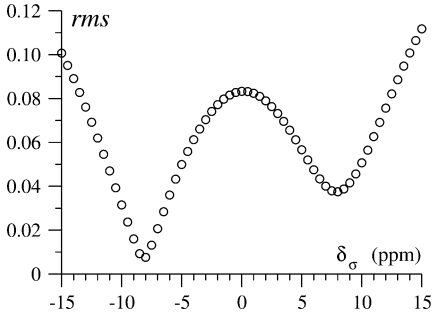

Figure 2. Plot of the rms deviation between experimental and simulated intensities for the ssbs in the ^{11}B MAS NMR spectrum of $NH_4B(C_6H_5)_4$ (Figure 1) as a function of the shift anisotropy (δ_σ). The rms values are obtained by least-squares optimization of C_Q to the experimental ssb intensities using fixed values for δ_σ (see text).

observed. To improve the precision of C_Q and δ_σ we have employed the constraint $\eta_Q = \eta_\sigma = 0.0$, imposed by the crystal structure, and thereby coincidence of the quadrupole coupling and CSA tensors. Moreover, the sign of the shift anisotropy has been confirmed by a number of optimizations of C_Q for fixed values of δ_σ in the range -15 to $+15$ ppm. The root-mean-square (rms) deviation between experimental and simulated ssb intensities from these optimizations is shown in Figure 2 as a function of δ_σ. Although this plot reveals two minima, it is evident that lowest rms is achieved for $\delta_\sigma \approx -8$ ppm, thereby confirming the negative sign of δ_σ. The isostructural tetraphenylborates $MB(C_6H_5)_4$ with the cations M = Na, K, Rb, and Cs have been investigated in a similar manner by slow-speed ^{11}B MAS NMR. The C_Q, δ_σ, and δ_{iso} parameters resulting from least-squares fitting to the ssb manifolds in these spectra are summarized in Table 1. The ^{11}B NMR data are very similar for the individual tetraphenylborates, which indicates that the cations only have a minor influence on the structure of the tetraphenylborate ion.

Datolite. The structure of datolite ($CaBSiO_4(OH)$) contains sheets of SiO_4 and BO_3OH tetrahedra that form four- and eight-membered rings where each BO_3OH tetrahedron is connected to three SiO_4 tetrahedra.[32,33] The Ca^{2+} ions are situated between the sheets, which are arranged parallel to the (100) plane. The ^{11}B MAS NMR spectrum of datolite, shown in Figure 3a, exhibits a manifold of ssbs from a single tetrahedrally coordinated ^{11}B site, in agreement with the crystal structure for this mineral.[32,33] The manifold of ssbs is quite symmetric; however, minor asymmetries are observed in the spectral regions for the outer edges (± 60 to ± 90 kHz), indicating the possible presence of a small CSA. Least-squares optimization to the ssbs from the satellite transitions gives the quadrupole coupling parameters and the isotropic chemical shift listed in Table 2 for datolite and results in a small, negative value for the shift anisotropy ($\delta_\sigma = -5 \pm 3$ ppm). However, the ssb intensities are insensitive to variations in η_σ and the Euler angles relating the CSA and quadrupole coupling tensors. Thus, employing $\eta_\sigma = 0.5$ and assuming coincidence of the CSA and quadrupole coupling tensors results in a simulated spectrum (Figure 3b) that reproduces the experimental ssb intensities in an excellent manner. To improve the precision of the somewhat uncertain ^{11}B CSA parameters, datolite is studied by ^{11}B SC NMR by employing a two-axis goniometer SC probe.[19] A typical ^{11}B SC NMR spectrum of datolite is shown in Figure 4a and illustrates the observation of four pairs of satellite transitions, whereas distinct resonances from the corresponding central transitions cannot be resolved. However, two of the pairs of satellites exhibit somewhat lower intensities as compared to the two other pairs. This indicates that the studied crystal of datolite

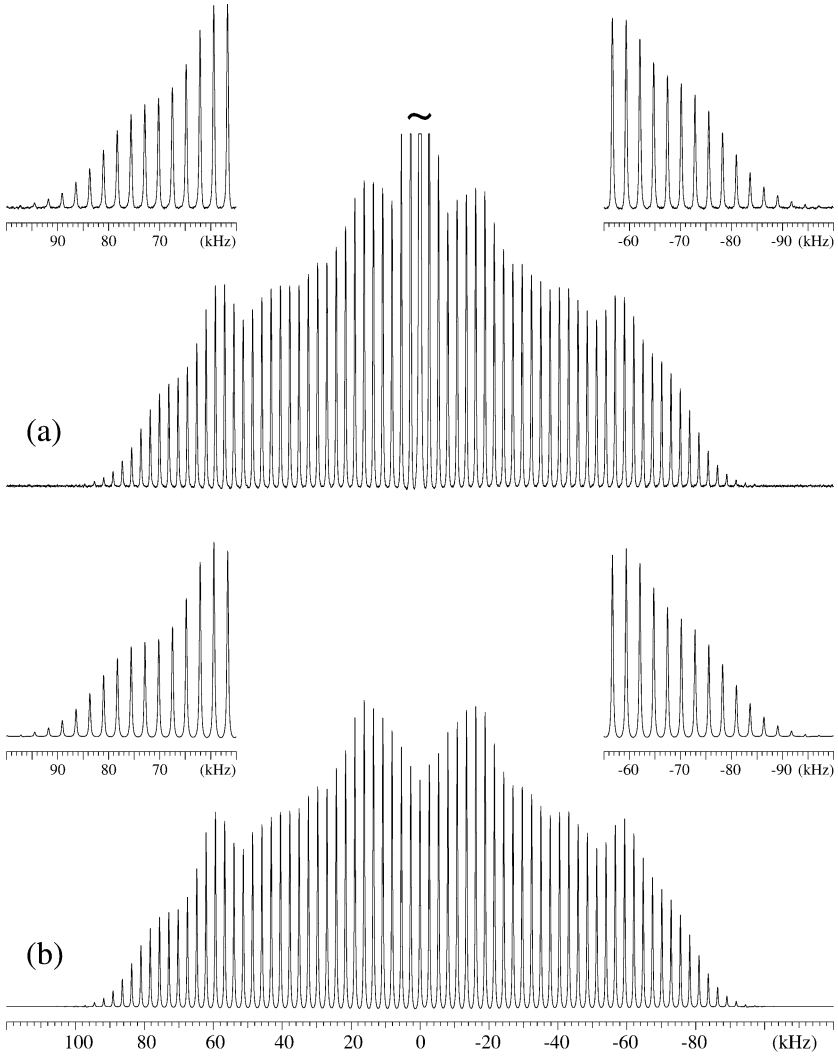

Figure 3. (a) ^{11}B MAS NMR spectrum showing the satellite transitions for datolite ($CaBSiO_4(OH)$), obtained using ^{1}H decoupling, $\nu_R = 2700$ Hz, a relaxation delay of 30 s, and 1024 scans. The center band and first-order ssbs from the central transition are cutoff at about $^1/_{12}$th of the total height for the centerband. (b) Optimized simulation of the satellite transitions in (a) corresponding to the ^{11}B parameters in Table 2 for datolite. The insets illustrate the small asymmetries in ssb intensities in the outer regions of the spectra.

TABLE 2: ^{11}B Quadrupolar Couplings (C_Q, η_Q), Chemical Shift Parameters (δ_σ, η_σ, δ_{iso}), and Relative Orientations (ψ; χ; ξ) of the Two Tensors from ^{11}B MAS, Single-Crystal,[a] and MQMAS NMR at 14.1 T

compound	site[b]	δ_{iso}[c] (ppm)	C_Q (MHz)	η_Q	δ_σ (ppm)	η_σ	ψ	χ	ξ	method
datolite	T	0.2 ± 0.2	0.17 ± 0.01	0.65 ± 0.02	-5 ± 3					MAS
($CaBSiO_4(OH)$)	T		0.172 ± 0.001	0.647 ± 0.005	-4.6 ± 0.4	0.4 ± 0.2	45 ± 15	7 ± 3	150 ± 20	SC
danburite	T	-0.2 ± 0.1	0.39 ± 0.02	0.43 ± 0.03						SC
($CaB_2Si_2O_8$)	T		0.392 ± 0.002	0.429 ± 0.004	6.0 ± 0.6	0.4 ± 0.1	0 ± 12	6 ± 3	135 ± 12	SC
colemanite	T_1	1.2 ± 0.2	0.440 ± 0.001	0.499 ± 0.003	6.4 ± 1.5	0.3 ± 0.1	64 ± 7	22 ± 4	105 ± 9	MAS
($CaB_3O_4(OH)_3 \cdot H_2O$)	T_2	1.2 ± 0.2	0.312 ± 0.001	0.809 ± 0.003	-4.3 ± 0.4	0.7 ± 0.2	33 ± 10	12 ± 4	120 ± 15	SC
	Δ	17.1 ± 0.3	2.543 ± 0.005	0.055 ± 0.004	-4.5 ± 0.5	0.8 ± 0.1	80 ± 5	87 ± 4	110 ± 5	SC
borax	T	2.1 ± 0.1	0.497 ± 0.001	0.624 ± 0.003	7.0 ± 0.5	0.7 ± 0.1	39 ± 8	12 ± 3	125 ± 9	SC
($Na_2B_4O_7 \cdot 10H_2O$)	Δ	18.2 ± 0.1	2.565 ± 0.003	0.105 ± 0.002	-3.4 ± 0.4	0.2 ± 0.2	44 ± 45	84 ± 3	81 ± 3	SC
$Li_2B_4O_7$	T	2.3 ± 0.1	0.52 ± 0.02	0.51 ± 0.02						MAS
	Δ	18.2 ± 0.2	2.56 ± 0.03	0.21 ± 0.04						MAS
	Δ				-12 ± 3	0.9 ± 0.1				MQMAS

[a] The CSA parameters and the Euler angles are determined from the sum frequencies for the satellite transitions in the SC NMR experiments. [b] Parameters for tetrahedral (T) and trigonal (Δ) coordinated boron. [c] Isotropic chemical shifts are in all cases determined from ^{11}B MAS NMR experiments.

contains two single crystals with different orientations. Thus, the ^{11}B SC NMR spectrum reveals the presence of two magnetically different ^{11}B sites in datolite in agreement with its monoclinic crystal structure[32,33] (space group $P2_1/c$ and $Z = 4$) where the four ^{11}B sites in pairs are related by inversion symmetry. In this work we have only analyzed the resonances from the two sets of satellite transitions with the largest intensities, originating from the dominant single crystal for our crystal of datolite. Figure 5a,b illustrates rotation plots for these two sets of satellite transitions corresponding to the two rotation

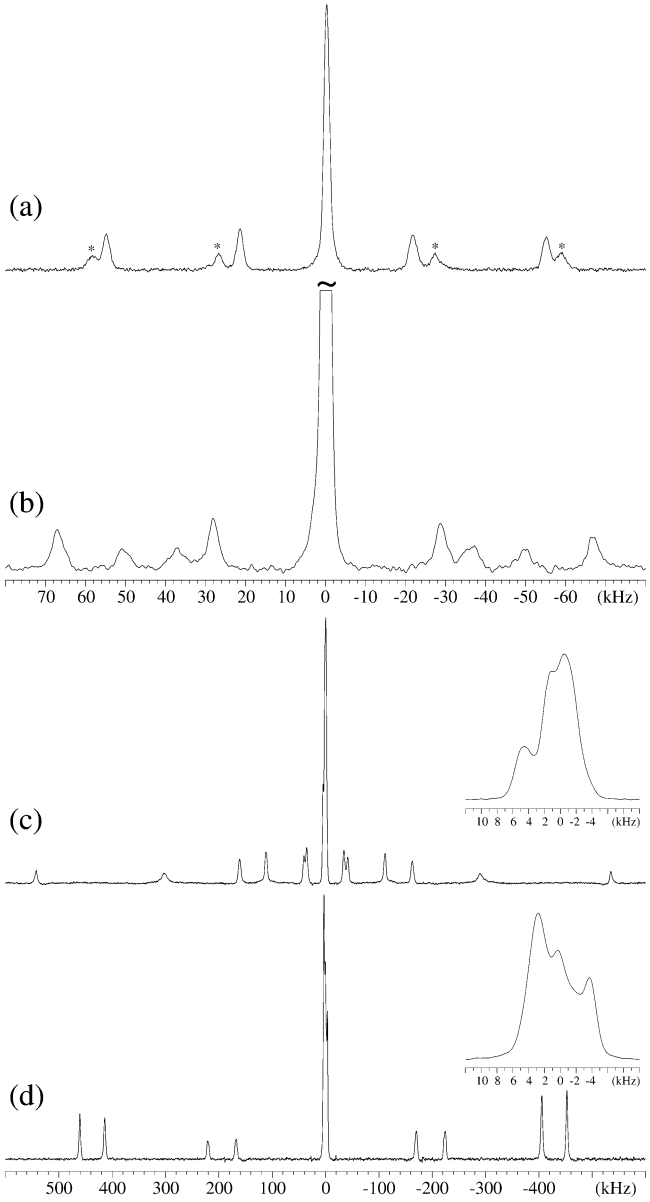

Figure 4. ^{11}B SC NMR spectra (14.1 T) of (a) datolite ($CaBSiO_4(OH)$), (b) danburite ($CaB_2Si_2O_8$), (c) colemanite ($CaB_3O_4(OH)_3 \cdot H_2O$), and (d) borax ($Na_2B_4O_7 \cdot 10H_2O$). The spectra in (a), (c), and (d) are recorded using ^{1}H decoupling. The asterisks in (a) indicate the resonances from the satellites for the smallest of the two single crystals in our crystal of datolite. The resonance from the central transition in (b) is cutoff at about one-third of its total height. The expansions in (c) and (d) illustrate the partly resolved resonances for the central transition from the magnetically different ^{11}B sites.

axes *a* and *b*. The rotation patterns for the two sites are quite similar, in agreement with the fact that the two sites are related by symmetry. Analysis of the rotation plots in Figure 5a,b, including the quadrupole coupling and CSA interactions, gives the quadrupole coupling parameters with high precision (Table 2) and a preliminary value for the shift anisotropy of $\delta_\sigma = -4.2 \pm 1.0$ ppm. However, determination of η_σ and the Euler angles relating the two tensors cannot be obtained from these rotation plots. The latter reflects the fact that the satellite transitions are strongly dominated by the quadrupole coupling interaction and that the BO_4 site in datolite only experiences a small CSA. An improved reflection of the ^{11}B CSA from the ^{11}B SC NMR spectra is achieved from the sum frequency of the resonances from the $m = {}^1/_2 \leftrightarrow m = {}^3/_2$ and $m = -{}^1/_2 \leftrightarrow m = -{}^3/_2$ transitions. This approach has earlier been employed in a ^{14}N

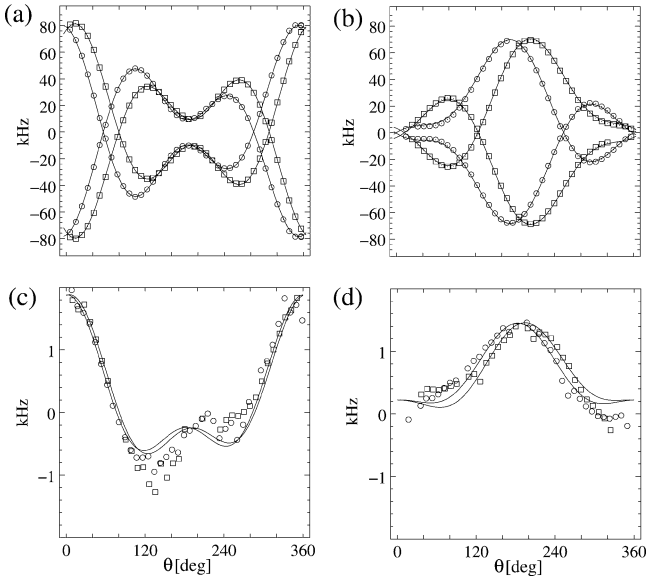

Figure 5. Rotation plots of the ^{11}B SC resonance frequencies from the satellite transitions for the two magnetically inequivalent B nuclei in datolite for rotation about (a) the *a* axis and (b) the *b* axis for the two-axis goniometer SC probe. The corresponding rotation plots of the sum frequencies for the $m = {}^1/_2 \leftrightarrow m = {}^3/_2$ and $m = -{}^1/_2 \leftrightarrow m = -{}^3/_2$ satellite transitions are shown in (c) and (d) for rotations about the *a* and *b* axes, respectively. The resonances for the two sites are marked by circles and squares, and the curves illustrate the best results from least-squares fitting to the resonance frequencies.

SC NMR study[34] and utilizes the fact that the sum frequencies are not affected by the first-order quadrupole coupling interaction but only the first-order CSA and the second-order quadrupole interactions. For the C_Q, η_Q parameters listed for datolite in Table 2 and the preliminary values for the CSA parameters $\delta_\sigma = -4.2$ ppm, $\eta_\sigma = 0.5$, simulations show that the second-order quadrupole interaction shifts the sum frequency over a spectral range of 40 Hz whereas the first-order CSA interaction gives shifts over a range of 2330 Hz at a magnetic field of 14.1 T. Thus, a rotation plot of the sum frequencies will be dominated by the CSA interaction, providing the basis for a more precise determination of the ^{11}B CSA parameters. Rotation plots of the sum frequencies for the two orientations (*a* and *b*) are illustrated in Figure 5c,d and show a variation in sum frequencies over a range of about 3.0 and 1.5 kHz for the rotations about the *a* and *b* axes, respectively. Analysis of these plots, including the first-order CSA, the second-order quadrupole interaction, and the quadrupole coupling parameters determined from the rotation plots in Figure 5a,b as fixed parameters, gives the CSA parameters listed in Table 2 for datolite and the simulated sum frequencies illustrated in Figure 5c,d. The simulated sum frequencies deviate somewhat from the experimental data in the regions $120° < \theta < 160°$ for the *a* axis and $280° < \theta < 360°$ for the *b* axis. These deviations of 100−400 Hz are ascribed to uncertainties in the determination of the frequencies for the satellite transitions, considering the line width of 1.5−2.0 kHz for these resonances. The ^{11}B NMR parameters and their error limits for datolite (Table 2) clearly reveal that the ^{11}B CSA and the relative orientation of the CSA and quadrupole tensors are determined with good precision from the sum frequencies for the satellite transitions in ^{11}B SC NMR.

Danburite. Danburite ($CaB_2Si_2O_8$) has an orthorhombic structure (space group *Pnam*, $Z = 4$) that consists of a continuous tetrahedral framework of alternating B_2O_7 and Si_2O_7 units where only the bridging B−O−B and Si−O−Si oxygen atoms of these units are situated in the mirror plane.[35] The latter

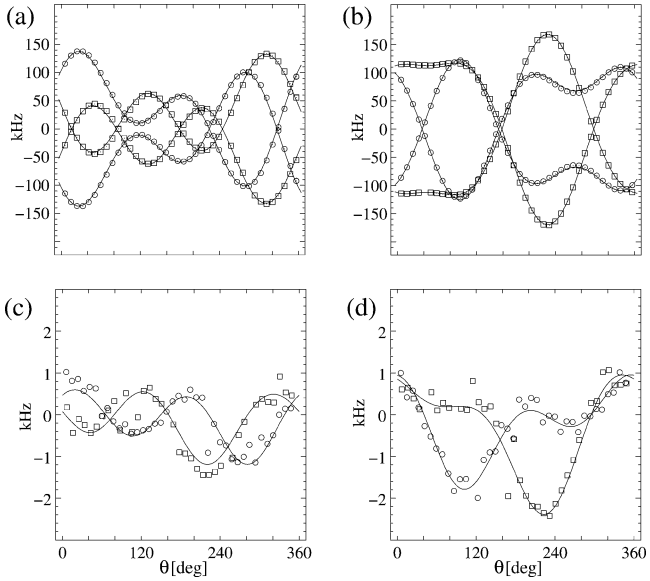

Figure 6. Rotation plots of the ^{11}B SC resonance frequencies from the satellite transitions for danburite ($CaB_2Si_2O_8$) for rotation about (a) the *a* axis and (b) the *b* axis. The corresponding rotation plots of sum frequencies for the $m = {}^1/_2 \leftrightarrow m = {}^3/_2$ and $m = -{}^1/_2 \leftrightarrow m = -{}^3/_2$ satellite transitions are shown in (c) and (d) for rotations about the *a* and *b* axes, respectively. For clarity, only rotation plots for two of the four magnetically nonequivalent ^{11}B sites are shown in this figure.

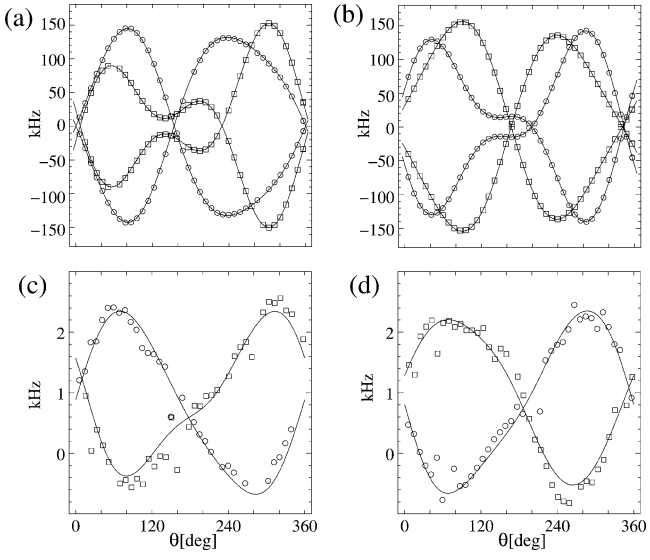

Figure 7. Rotation plots of the ^{11}B SC resonance frequencies from the satellite transitions for one of the two inequivalent BO_4 sites in colemanite ($CaB_3O_4(OH)_3{\cdot}H_2O$) for rotations about (a) the *a* axis and (b) the *b* axis. (c) and (d) illustrate rotation plots of sum frequencies for the satellite transitions for the same BO_4 site for rotations about the *a* and *b* axes, respectively. The solid curves show the result from least-squares fitting to the resonance frequencies, employing the ^{11}B NMR paramaters for the tetrahedral T_2 site in colemanite (Table 2).

implies that the local symmetry of the B sites does not impose any constraints on the Euler angles relating the ^{11}B quadrupole coupling and CSA tensors. The ^{11}B MAS NMR spectrum of danburite (14.1 T, $\nu_R = 3.0$ kHz, not shown) displays a highly symmetric manifold of ssbs from the satellite transitions, which extends over a spectral range of 425 kHz. Least-squares fitting to this manifold gives the quadrupole coupling parameters in Table 2 for danburite. These data show that the ^{11}B site in danburite experiences a quadrupole coupling that is about twice the magnitude of the C_Q value for the ^{11}B site in datolite. The stronger quadrupole coupling interaction as compared to the C_Q value for datolite, combined with a comparison of the experimental and simulated spectra for the satellite transitions for danburite (not shown), implies that effects from a small CSA ($|\delta_\sigma| \lesssim 10$ ppm) cannot be retrieved from the MAS NMR spectrum (14.1 T). In accord with the crystal structure for danburite,[35] the ^{11}B SC NMR spectra of a single crystal of danburite (Figure 4b) allow distinction of resonances for four sets of satellite transitions from four magnetically nonequivalent ^{11}B sites. Optimization to the rotation plots of frequencies for the four sets of satellites (Figure 6a,b) gives the quadrupole coupling parameters (Table 2) and a shift anisotropy of $\delta_\sigma = 5 \pm 3$ ppm, whereas values for η_σ and the Euler angles (ψ, χ, ξ) cannot be reliably obtained. An improved determination of the ^{11}B CSA is achieved from the rotation plots of sum frequencies for the satellite transitions, as illustrated in Figure 6c,d. Least-squares analysis of the variation in sum frequencies in these plots, employing the C_Q and η_Q values determined from the satellite transitions (Figure 6a,b) as fixed parameters, gives the CSA parameters and Euler angles in Table 2 for danburite. These data show that the magnitude of the CSA in danburite and datolite are very similar; however, the precision of these parameters and of the Euler angles (ψ, χ, ξ) is slightly improved for danburite. This reflects the stronger ^{11}B quadrupole coupling for danburite, because the determination of the relative orientation of the two tensors is based on the second-order quadrupolar interaction. We note that the ^{11}B quadrupole coupling parameters $C_Q = 0.412$ MHz and $\eta_Q = 0.45$ were reported for danburite in an early ^{11}B SC NMR study.[15]

Colemanite. Colemanite ($CaB_3O_4(OH)_3{\cdot}H_2O$) is an inoborate mineral that crystallizes in the monoclinic space group $P2_1/a$.[36] The basic building unit in colemanite is a ring of composition $[B_3O_5(OH)_3]^{4-}$, which includes two BO_4 tetrahedra and a trigonal BO_3 site. The ^{11}B MAS NMR spectrum of colemanite (not shown) displays the characteristic second-order quadrupolar line shape for the central transition from the BO_3 site and overlapping centerbands and ssbs for the two crystallographically distinct BO_4 sites. The latter impedes a straightforward determination of the quadrupole coupling parameters for the two tetrahedral sites and shows that these sites possess very similar isotropic chemical shifts. An improved reflection of the two different BO_4 environments is achieved from the ^{11}B SC NMR spectra (Figure 4c) where resonances from the satellite transitions for four magnetically different BO_4 sites are observed in addition to the satellite transitions for two BO_3 sites (vide supra). Least-squares analysis of the rotation plots for these satellites (Figure 7a,b) gives the quadrupole coupling parameters with high precision whereas the CSAs and the (ψ, χ, ξ) Euler angles are derived from the analysis of the sum frequencies for the satellites (Figure 7c,d). The optimized parameters (Table 2) reveal that the main difference in ^{11}B data for the two sites is the values of the asymmetry parameters and the sign of the shift anisotropy, whereas the Euler angles show that the two tensors exhibit nearly the same relative orientation for the two BO_4 tetrahedra. The quadrupole coupling parameters are in good agreement with those reported in an early ^{11}B SC NMR study (i.e., $C_Q = 0.436$ MHz, $\eta_Q = 0.487$ and $C_Q = 0.309$ MHz, $\eta_Q = 0.825$).[14]

Borax. $Na_2B_4O_7{\cdot}10H_2O$ (borax) crystallizes in the monoclinic space group $C2/c$ and includes tetraborate units linked together by hydrogen bonds. From the crystal structure[37] and ^{11}B MAS NMR,[10] it is well-known that borax contains two different ^{11}B sites possessing trigonal and tetrahedral coordination. A ^{11}B SC NMR analysis of borax results in the rotation plots for the

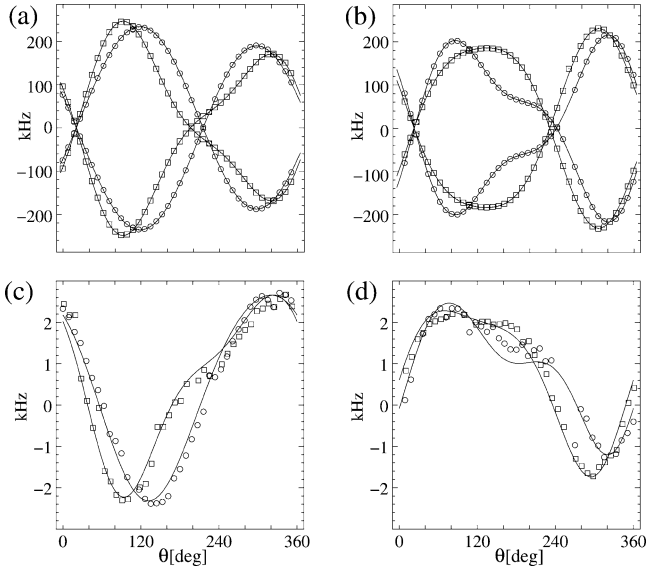

Figure 8. Rotation plots of the ^{11}B SC resonance frequencies from the satellite transitions for the BO_4 site in borax ($Na_2B_4O_7 \cdot 10H_2O$) for rotations about (a) the *a* axis and (b) the *b* axis. The corresponding rotation plots of sum frequencies for the satellite transitions are shown in (c) and (d).

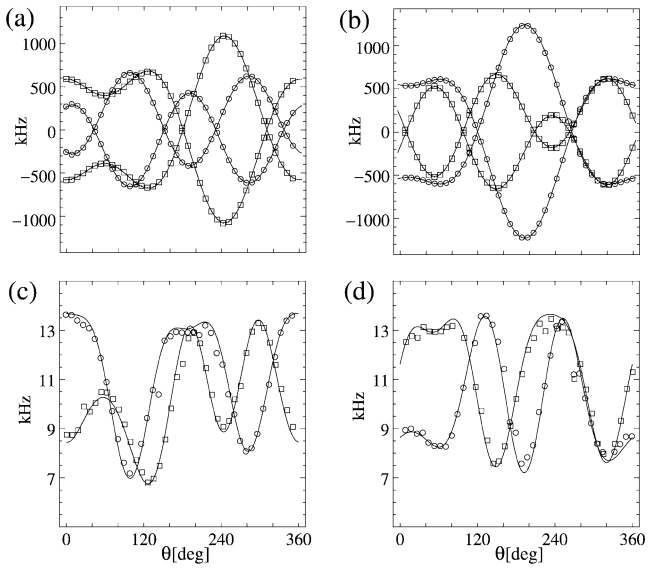

Figure 9. Rotation plots of the ^{11}B SC resonance frequencies from the satellite transitions for the trigonal boron site in borax ($Na_2B_4O_7 \cdot 10H_2O$) for rotations about (a) the *a* axis and (b) the *b* axis. (c) and (d) illustrate the corresponding plots of sum frequencies for the satellite transitions.

satellite transitions shown in Figure 8a,b for the two magnetically inequivalent BO_4 sites. Least-squares optimization to the frequencies for these transitions gives the quadrupole coupling parameters listed in Table 2 for the BO_4 site. The ^{11}B CSA parameters and the Euler angles (ψ, χ, ξ) are obtained from the rotation plots of sum frequencies in Figure 8c,d. The ^{11}B CSA is slightly larger than those observed for the BO_4 sites in the other minerals studied by ^{11}B SC NMR. Overall, our results indicate that ^{11}B shift anisotropies in the range $|\delta_\sigma| \lesssim 10$ ppm are expected for tetrahedrally coordinated boron in borates. This range is somewhat smaller than the δ_σ values reported for trigonal BO_3 sites in borates (i.e., $|\delta_\sigma| \lesssim 22$ ppm).[9]

Trigonal BO_3 Sites. Although this work primarily focuses on boron in tetrahedral coordination, the anisotropic ^{11}B NMR parameters for the BO_3 sites in colemanite and borax (Table 2) have also been determined from the ^{11}B SC NMR spectra. Despite the fact that these sites exhibit stronger quadrupole couplings and second-order quadrupolar line shapes of the central transition in the ^{11}B MAS spectra at 14.1 T, the overlap of resonances from the central transitions for the magnetically different BO_3 sites in the SC NMR spectra (Figure 4c,d) prevent a determination of the ^{11}B parameters from analysis of the central transitions alone. Thus, the satellite transitions and the same approach as used for the tetrahedrally coordinated ^{11}B sites are employed as illustrated in Figure 9 for the BO_3 site in borax. For this site, the sum frequencies for the satellite transitions (Figure 9c,d) exhibit a larger variation in frequency as compared to those observed for the BO_4 sites. The increased variation in these frequencies reflects a larger effect from the second-order quadrupolar interaction and results in an excellent agreement between the experimental and simulated sum frequencies. It is noted that the ^{11}B shift anisotropies for the trigonal BO_3 sites in borax and colemanite (Table 2) are smaller than the corresponding values observed for the BO_4 sites in these minerals.

^{11}B CSA from MQMAS NMR ($Li_2B_4O_7$). For $Li_2B_4O_7$ it was not possible to obtain a single crystal of a sufficient size for SC NMR. Thus, a powdered sample has initially been investigated by ^{11}B MAS NMR of the central and satellite transitions (spectra not shown), which gives the C_Q, η_Q, and δ_{iso} values for the BO_3 and BO_4 sites listed in Table 2 for $Li_2B_4O_7$. The observation of a BO_3 and BO_4 site is in accord with the crystal structure reported for $Li_2B_4O_7$.[38] The possibility of obtaining small ^{11}B CSAs from MQMAS NMR experiments is investigated in Figure 10 by the ^{11}B MQMAS NMR spectrum of $Li_2B_4O_7$. This experiment utilizes the fact that the CSA interaction is scaled by the multiple-quantum order in the isotropic dimension of the MQMAS spectrum. This may result in an improved precision of the CSA parameters, determined from the spinning sideband intensities in the isotropic dimension of the MQMAS spectrum, as recently demonstrated for other half-integer spin quadrupolar nuclei.[39−41] The ^{11}B MQMAS NMR spectrum of $Li_2B_4O_7$ is obtained by using the three-pulse shifted-echo sequence.[42,43] This sequence is chosen because theoretical calculations and experiments show that selection of the $-3Q \rightarrow +1Q$ ($\Delta p = 4$) coherence transfer pathway for the mixing pulse (i.e., the second pulse) reduces contributions from rf-induced spinning sidebands to the ssb manifolds in the isotropic dimension, a condition that holds for $\omega_Q \gg \omega_{rf}$, where $\omega_Q = C_Q/[2I(2I-1)]$.[44] Moreover, it is not expected that ^{11}B−^{11}B dipolar couplings make any significant contribution to the ssb intensities in the isotropic dimension, considering the shortest ^{11}B−^{11}B distance of 2.5 Å in $Li_2B_4O_7$ and the spinning speed ($\nu_R = 5.0$ kHz) employed for the MQMAS experiment. In accordance with the ^{11}B MAS NMR spectrum and the crystal structure for $Li_2B_4O_7$,[38] the ^{11}B MQMAS NMR spectrum of $Li_2B_4O_7$ displays resonances from a trigonal and a tetrahedral boron site with the approximate chemical shifts of 15 and 3 ppm in the anisotropic (F2) dimension, respectively. Summation of the ssb manifolds in the isotropic dimension over the +1, 0, and −1 order ssbs in the anisotropic dimension, using the approach by Wang et al.,[39] gives the reconstructed ssb manifold for the trigonal boron site shown in Figure 10b. Simulation of this spectrum, considering the first-order CSA interaction only, results in the parameters $\delta_\sigma = -12 \pm 3$ ppm and $\eta_\sigma = 0.9 \pm 0.1$ and the optimized simulation shown in Figure 10c. This value for the shift anisotropy is slightly larger than those determined for the BO_3 sites in borax and colemanite (Table 2) but of the same magnitude as those reported for trigonal ^{11}B

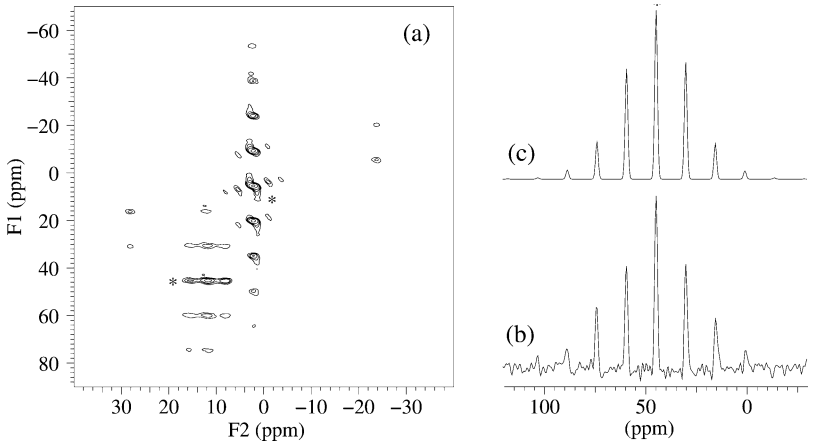

Figure 10. (a) Contour plot of the ^{11}B MQMAS NMR spectrum ($\nu_R = 5.0$ kHz, 14.1 T) for $Li_2B_4O_7$ recorded using the three-pulse shifted-echo sequence, a spectral width of 75 kHz in both dimensions, 128 t_1 increments, a relaxation delay of 37 s, and 24 scans. The asterisks indicate the isotropic peaks for the BO_3 and BO_4 sites. (b) Reconstructed summation of the ssb intensities in the isotropic dimension of the MQMAS spectrum for the BO_3 site (see text). (c) Optimized simulation of the spectrum in (b), considering the scaled CSA interaction in the MQMAS experiment and corresponding to the ^{11}B CSA parameters listed in Table 2 for $Li_2B_4O_7$.

sites in anhydrous tetraborates.[9] A similar analysis of the ssbs observed for the tetrahedral site did not result in a reliable determination of the CSA parameters. This may reflect the fact that the condition $\omega_Q \gg \omega_{rf}$ is not fulfilled for the tetrahedral site, which possesses a small quadrupole coupling (cf. Table 2). Thus, the ssb intensities for this site are somewhat distorted by rf-induced contributions resulting from modulations of the first-order quadrupole interaction.[45]

Conclusions

The present solid-state ^{11}B NMR study of tetraphenyl borates, datolite, danburite, colemanite, borax, and $Li_2B_4O_7$ has shown that tetrahedrally coordinated boron in these borates possess ^{11}B shift anisotropies ($\delta_\sigma = \delta_{iso} - \delta_{zz}$) of the order $|\delta_\sigma| \lesssim 10$ ppm. For small ^{11}B quadrupole couplings (i.e., $C_Q \lesssim 0.2$ MHz) the effect from the chemical shift anisotropy (CSA) can be observed in ^{11}B MAS NMR spectra of the satellite transitions at 14.1 T. This allows determination of the CSA and quadrupole coupling parameters from optimization to the manifold of spinning sidebands. For strong quadrupole couplings, e.g., trigonal BO_3 sites, the ^{11}B CSAs can be extracted from the spinning sidebands in the isotropic dimension of ^{11}B MQMAS NMR spectra, as illustrated for the BO_3 site in $Li_2B_4O_7$. However, improved precision for the ^{11}B CSA parameters and the Euler angles, describing the relative orientation of the CSA and quadrupole coupling tensors, is obtained from single-crystal NMR spectra of the satellite transitions. The optimum precision is achieved by analysis of the sum frequencies for the $m = {}^1/_2 \leftrightarrow m = {}^3/_2$ and $m = -{}^1/_2 \leftrightarrow m = -{}^3/_2$ transitions because these frequencies are influenced by only the first-order CSA and the second-order quadrupolar coupling interaction.

Acknowledgment. The use of the facilities at the Instrument Centre for Solid-State NMR Spectroscopy, University of Aarhus, sponsored by the Danish Natural Science Research Council, the Danish Technical Science Research Council, Teknologistyrelsen, Carlsbergfondet, and Direktør Ib Henriksens Fond, is acknowledged. J.S. thanks the Danish Natural Science Research Council (J. No. 0001237) and T.V. Carlsbergfondet for financial support. Richard Wilson, Department of Geology, University of Aarhus, and Ole Johnsen, the Geological Museum, University of Copenhagen, are acknowledged for providing the mineral samples of datolite, danburite, and colemanite.

References and Notes

(1) Silver, A. H.; Bray, P. J. *J. Chem. Phys.* **1958**, *29*, 984.
(2) Bray, P. J.; Edwards, J. O.; O'Keefe, J. G.; Ross, V. F.; Tatsuzaki, I. *J. Chem. Phys.* **1961**, *35*, 435.
(3) Bray, P. J. *Inorg. Chim. Acta* **1999**, *289*, 158.
(4) Turner, G. L.; Smith, K. A.; Kirkpatrick, R. J.; Oldfield, E. *J. Magn. Reson.* **1986**, *67*, 544.
(5) Müller, D.; Grimmer, A. R.; Timper, U.; Heller, G.; Shakibai-Moghadam, M. *Z. Anorg. Allg. Chem.* **1993**, *619*, 1262.
(6) van Wüllen, L.; Müller-Warmuth, W.; Papageorgiou, D.; Pentinghaus, H. J. *J. Non-Cryst. Solids* **1994**, *171*, 53.
(7) Stebbins, J. F.; Zhao, P.; Kroecker, S. *Solid State Nucl. Magn. Reson.* **2000**, *16*, 9.
(8) Martens, R.; Müller-Warmuth, W. *J. Non-Cryst. Solids* **2000**, *265*, 167.
(9) Kroeker S.; Stebbins, J. F. *Inorg. Chem.* **2001**, *40*, 6239.
(10) Dec, S. F.; Maciel, G. E. *J. Magn. Reson.* **1990**, *87*, 153.
(11) van Wüllen, L.; Müller-Warmuth, W. *Solid State Nucl. Magn. Reson.* **1993**, *2*, 279.
(12) Jäger, C.; Herzog, K.; Thomas, B.; Feike, M.; Kunath-Fandrei, G. *Solid State Nucl. Magn. Reson.* **1995**, *5*, 51.
(13) Fyfe, C. A.; Skibsted, J.; Schwieger, W. *Inorg. Chem.* **2001**, *40* 5906.
(14) Holuj, F.; Petch, H. E. *Can. J. Phys.* **1960**, *38*, 515.
(15) Brun, E.; Ghose, S. *J. Chem. Phys.* **1964**, *40*, 3031.
(16) Bryce, D. L.; Wasylishen, R. E.; Gee, M. *J. Phys. Chem. A* **2001**, *105*, 3633.
(17) Forgeron, M. A. M.; Bryce, D. L.; Wasylishen, R. E.; Rösler, R. *J. Phys. Chem. A* **2003**, *107*, 726.
(18) Schurko, R. W.; Hung, I.; Schauff, S.; Macdonald, C. L. B.; Cowley, A. H. *J. Phys. Chem. A* **2002**, *106*, 10096.
(19) Vosegaard, T.; Hald, E.; Daugaard, P.; Jakobsen, H. J. *Rev. Sci. Instrum.* **1999**, *70*, 1771.
(20) Vosegaard, T.; Daugaard, P.; Hald, E.; Jakobsen, H. J. *J. Magn. Reson.* **2000**, *142*, 379.
(21) Vosegaard, T.; Hald, E.; Langer, V.; Skov, H. J.; Daugaard, P.; Bildsøe, H.; Jakobsen, H. J. *J. Magn. Reson.* **1998**, *135*, 126.
(22) Skibsted, J.; Nielsen, N. C.; Bildsøe, H.; Jakobsen, H. J. *J. Am. Chem. Soc.* **1993**, *115*, 7351.
(23) Vosegaard, T.; Skibsted, J.; Bildsøe, H.; Jakobsen, H. J. *J. Magn. Reson. Ser. A* **1996**, *122*, 111.
(24) Skibsted, J.; Nielsen, N. C.; Bildsøe, H.; Jakobsen, H. J. *J. Magn. Reson.* **1991**, *95*, 88.
(25) Skibsted, J.; Nielsen, N. C.; Bildsøe, H.; Jakobsen, H. J. *Chem. Phys. Lett.* **1992**, *188*, 405.
(26) Skibsted, J.; Vosegaard, T.; Bildsøe, H.; Jakobsen, H. J. *J. Phys. Chem.* **1996**, *100*, 14872.
(27) Bak, M.; Rasmussen, J. T.; Nielsen, N. C. *J. Magn. Reson.* **2000**, *147*, 296.
(28) Bak, M.; Schultz, R.; Vosegaard, T.; Nielsen, N. C. *J. Magn. Reson.* **2002**, *154*, 28.
(29) Vosegaard, T.; Malmendal, A.; Nielsen, N. C. *Chem. Monthly* **2002**, *133*, 1555.
(30) Dewar, M. J. S.; Jones, R. *J. Am. Chem. Soc.* **1967**, *89*, 2408.
(31) Steiner, T.; Mason, S. A. *Acta Crystallogr. B* **2000**, *56*, 254.

(32) Ito, T.; Mori, H. *Acta Crystallogr.* **1953**, *6*, 24.
(33) Foit, F. F.; Phillips, M. W.; Gibbs, G. V. *Am. Mineral.* **1973**, *58*, 909.
(34) Bastow, T. J.; Stuart, S. N. *Chem. Phys. Lett.* **1991**, *180*, 305.
(35) Phillips, M. W.; Gibbs, G. V.; Ribbe, P. H. *Am. Mineral.* **1974**, *59*, 79.
(36) Burns, P. C.; Hawthorne, F. C. *Can. Mineral.* **1993**, *31*, 297.
(37) Levy H. A.; Lisensky, G. C. *Acta Crystallogr.* **1987**, *B34*, 3502.
(38) Radaev, S. F.; Muradyan, L. A.; Malakhova, L. F.; Burak, Y. V.; Simonov, V. I. *Sov. Phys. Crystallogr.* **1989**, *34*, 842.
(39) Wang, S. H.; Xu, Z.; Baltisberger, J. H.; Bull, L. M.; Stebbins, J. F.; Pines, A. *Solid State Nucl. Magn. Reson.* **1997**, *8*, 1.
(40) Nielsen, U. G.; Jakobsen, H. J.; Skibsted, J. *Solid State Nucl. Magn. Reson.* **2000**, *20*, 23.
(41) Nielsen, U. G.; Jakobsen, H. J.; Skibsted, J. *Solid State Nucl. Magn. Reson.* **2003**, *23*, 107.
(42) Massiot, D.; Touzo, B.; Trumeau, D.; Coutures, J. P.; Virlet, J.; Florian, P.; Grandinetti, P. J. *Solid State Nucl. Magn. Reson.* **1996**, *6*, 73.
(43) Vosegaard, T.; Florian, P.; Grandinetti, P. J.; Massiot, D. *J. Magn. Reson.* **2000**, *143*, 217.
(44) Vosegaard, T.; Massiot, D.; Grandinetti, P. J. *Exp. NMR Conf., 41st* (Asilomar, CA) **2000**, Poster M T 303.
(45) Marinelli, L.; Frydman, L. *Chem. Phys. Lett.* **1997**, *275*, 188.